Journal of Catalysis **211,** 252–264 (2002)
doi:10.1006/jcat.2002.3734

Gallium–Hydrogen Bond Formation on Gallium and Gallium–Palladium Silica-Supported Catalysts

Sebastián E. Collins,* Miguel A. Baltanás,* José L. Garcia Fierro,† and Adrian L. Bonivardi*,[1]

*Instituto de Desarrollo Tecnológico para la Industria Química (CONICET, FIQ-UNL), Güemes 3450, 3000 Santa Fe, Argentina; and †Instituto de Catálisis y Petroleoquímica (CSIC), Cantoblanco, 28049 Madrid, Spain

Received April 15, 2002; revised June 27, 2002; accepted June 27, 2002

The interaction of H_2 with Ga/SiO_2, Pd/SiO_2, and $Ga–Pd/SiO_2$ catalysts has been investigated by *in situ* X-ray photoelectron and transmission infrared spectroscopies (XPS and FTIR). The precursors, calcined in dry air at 673 K, yield PdO and Ga_2O_3. Upon exposure to hydrogen reduction at 423 K, the fraction of reduced gallium ions ($Ga^{\delta+}$ cations, $\delta < 2$) was 16% on Ga-promoted Pd/SiO_2, whereas no Ga^{3+} was reduced over Ga/SiO_2 materials. It is suggested that this promotional reduction effect of the noble metal over gallium(III) is accomplished through hydrogen spillover from metallic palladium, early reduced at 423 K. Higher reduction temperatures (723 K) lead to highly dispersed metallic palladium crystallites on the catalysts surface, and to the reduction of about 23–28% of the total gallium content in both the Ga/SiO_2 and the $Ga–Pd/SiO_2$ materials. Above 473 K and under hydrogen flow, a band at 2020 cm^{-1} developed over all these reduced gallium-containing catalysts, which was assigned to $Ga^{\delta+}$–H bond stretching. A linear relationship was found between the intensity of this infrared signal and the total gallium or $Ga^{\delta+}$ loading over the catalysts, at 723 K and 760 Torr of flowing H_2. We propose that gallium–hydrogen bond formation can be achieved on Ga/SiO_2 by heterolytic hydrogen dissociation on the $Ga^{\delta+}$ cations, which are stabilized on the silica surface, to yield additional GaO–H bonds. In the $Ga–Pd/SiO_2$ catalysts the process is further aided by the metal particles. The $Ga^{\delta+}$–H species were unstable below 450 K and/or decomposed under evacuation but could be immediately regenerated after restoring H_2 pressure. The impact of the formation of this gallium–hydrogen bond over the hydrogenation of carbon dioxide to oxygenated compounds is also discussed.

Key Words: **gallium–hydrogen bond; palladium-based catalysts; Ga_2O_3 reduction; hydrogen dissociation; CO_2 hydrogenation; methanol synthesis.**

INTRODUCTION

The catalytic properties of gallium have received renewed attention from the mid-1980s. For example, there has been steadily growing interest in the investigation of the nature of the active sites on ZSM-5 zeolites modified with gallium, because aromatization of light alkanes can be accomplished by these catalysts (1–5). Discussions of research teams go from the role of Ga atoms or GaO_x oxides in the lattice on the depression of the protonic acidity of the zeolite to the formation of active forms of reduced gallium, such as Ga(I) or GaH_x monomeric species (6–10).

More recently, deep effects on the catalytic properties for achieving highly effective conversion of carbon dioxide to valuable compounds using composite catalysts which incorporate gallium oxide(s) and precious metals have been reported (11–13). Inui concluded that the reduced state of those catalysts that showed optimum catalytic properties could be controlled by a combination of direct and inverse hydrogen spillover from the noble metal and gallium sites, respectively (11). The development of an active Pd/Ga_2O_3 catalysts for the synthesis of methanol from CO_2 hydrogenation, able to compete with the classical Cu/ZnO formulation, was first reported by Fujitani *et al.* (12). Later on, Bonivardi *et al.* showed that gallium addition to Pd/SiO_2 catalysts produced a dramatic enhancement of the catalytic performance to give oxygenated compounds from the hydrogenation of carbon dioxide (13): Going from pure Pd/SiO_2 to Ga-promoted Pd/SiO_2, with a variable Ga-to-Pd atomic ratio, the initial activity to methanol improved from 1.7×10^{-3} to 4.5×10^{-1} s^{-1} at 523 K and 3 MPa (CO_2/H_2). Under the same reaction conditions, the initial selectivity to methanol went up to 62% for one of the gallium-promoted catalysts, compared to 17% over clean palladium/silica. Based on preliminary results of temperature-programmed reduction, these last authors proposed that palladium crystallites interacting with reduced gallium species could account for the unusual catalytic performance of the $Ga–Pd/SiO_2$ system. A mechanism involving intermediates from adsorbed CO_2 rather than CO, similar to those sustained for Cu/ZnO, was suggested since only traces of methanol were synthesized from CO/H_2 mixtures.

The impact of hydrogen activation in the hydrogenation of carbon oxides over these gallium-containing catalysts was not discussed in the mentioned works, probably because Ga is not as good a hydrogenation catalyst as the noble metals are and, actually, is not a widely employed catalytic element (11–13). In like manner, although it is

[1] To whom correspondence should be addressed. Fax: +54(342)4550944. E-mail: aboni@intec.unl.edu.ar.

0021-9517/02 $35.00

well-known that zinc oxide is able to activate dissociatively the hydrogen molecule (14–16), this point has not been further emphasized or considered in studies of methanol synthesis on the traditional Cu/ZnO catalysts, as it has been in the case of propane dehydrocyclization on Ga/H–ZMS-5 (7–10).

In this context, it is imperative to balance the knowledge of the chemistry of all the elemental components of a catalytic material, starting from molecular activation processes. Thus, the aim of this work is to furnish evidence of the chemistry of gallium species under reducing conditions in the hope that it will help in understanding the reaction pathways to oxygenated compounds from CO_2 and H_2. For this purpose, we report here our results on hydrogen interaction with Ga/SiO_2 and $Ga–Pd/SiO_2$ materials, followed by XPS and FTIR spectroscopies.

EXPERIMENTAL

Catalysts

Davison Grade 59 silica gel (W. R. Grace) was previously crushed and sieved through an 80-mesh Tyler screen. Next, the silica was purified, calcined in air at 773 K for 12 h, and characterized before being used as support for the catalysts, as described in (17) (average particle diameter = 52 μm; specific surface = 301 m^2/g; average pore diameter = 16 nm).

Catalysts with 2 wt% Pd loading were obtained via ion exchange of palladium acetate (Sigma, 99.97%), at pH 11 in $NH_4OH_{(aq)}$, onto the support. The exchanged material was washed at the same pH, and the supported tetrammine palladium complex was decomposed to diammine palladium on silica by drying at 423 K for 2 h under flowing air (200 cm^3/min), in a glass reactor (18). Then, different amounts of $Ga(NO_3)_3 \cdot xH_2O$ (Strem Chemicals, 99.99% Ga), in aqueous solution, were added by incipient wetness impregnation to the $[Pd(NH_3)_2]^{2+}/SiO_2$ at 3 Torr of N_2 (1 Torr = 133.3 Pa) and ambient temperature, in a rotary evaporator. Subsequently, the solids were frozen in liquid nitrogen and water was removed by sublimation at 3 Torr of N_2 to give dry *precursors*. The resulting precursors were then calcined in flowing air (200 cm^3/min) by heating from 298 to 673 K (2 h) at 2 K/min, to obtain palladium and gallium oxides on the SiO_2 surface (*calcined catalysts*). Last, portions of each calcined catalyst were reduced in a 5% H_2/Ar mixture (200 cm^3/min), heating from 298 to 723 K (2 h) at 2 K/min, to obtain the *prereduced catalysts*. Before removing these reduced catalysts from the glass reactor, they were passivated at 298 K by flowing O_2/Ar mixtures (200 cm^3/min) with increasing O_2 content, from 0.1 to 5% v/v. Blank samples of gallium/silica and palladium/silica were also prepared following the same procedure.

Table 1 summarizes the catalysts' codes and the main features of the reduced samples used in this work. The specific surface area of the catalysts was measured by the BET method (N_2), in a Micromeritics Acusorb 2000 apparatus. The fraction of exposed metallic palladium was determined by chemisorption of carbon monoxide pulses. Nonchemisorbed CO was hydrogenated to methane, which was then detected by a flame ionization detector, as described in (19). A JEOL 100 CX electron microscope operating in the bright-field mode was used to perform TEM characterization. X-ray diffraction spectrometry was employed over a selected set of the catalysts, using a Rich–Seifert JSO-Debyeflex 2002 diffractometer equipped with a Ni-filtered Cu $K\alpha$ radiation source.

TABLE 1

Surface Specific Area and Metallic Dispersion of the Prereduced Catalysts Versus Gallium and/or Palladium Content

Catalyst type[a]	Code	Pd (wt%)	Ga (wt%)	Ga-to-Pd atomic ratio (atom to atom)	BET surface area (m^2/g)	FE[b]	d_{Pd}[c] (nm)
Ga/SiO_2	Ga40	—	4.9	—	289	—	—
	Ga80	—	9.2[d]	—	257	—	—
Pd/SiO_2	PdGa00	2	—	0	292	58	1.4
$Ga–Pd/SiO_2$	PdGa20	2	2.6	2	—	45	1.4
	PdGa40	2	4.9	4	264	12	1.8
	PdGa80	2	9.2[d]	8	253	6	1.9

[a] Support: Davison G59 silica (BET surface area = 301 m^2/g; average pore diameter = 16 nm).

[b] Fraction of exposed metallic palladium, measured by CO pulses.

[c] Volume-to-area average diameter of palladium crystallites, as measured by TEM = $\Sigma n_i d_i^3 / \Sigma n_i d_i^2$.

[d] Loading equivalent to a monolayer of Ga_2O_3 onto the SiO_2 support.

XPS Apparatus and Procedures

Samples of either precursors or prereduced catalysts were ground and placed on a metallic sample holder. The samples were treated *in situ* in a pretreatment chamber. The precursors were first calcined at 673 K in 400 Torr of static O_2 for 30 min and were sequentially reduced *in situ* at 423, 573, and 723 K in 400 Torr of static H_2, for 30 min each time. The prereduced catalysts were re-reduced *in situ* at 523 K, under the same final conditions. After each treatment, the samples were degassed and directly transferred without exposure to air to an attached XPS analysis chamber. A VG Escalab 200R X-ray photoelectron spectrometer with a Mg $K\alpha_{1,2}$ source (incident energy of 1253.6 eV) and a hemispherical electron analyzer was used. The residual pressure in the ion-pumped analysis chamber was maintained below 3×10^{-9} Torr during data acquisition. C 1s, O 1s, O 2s, Ga 3d, Si 2p, Pd 3d, Ga 3d, and Ga LMM signals were recorded.

The electron-binding-energy scale was calibrated by assigning 532.6 eV to the O 1s peak. The binding energies reported here are accurate to ±0.1 eV, with the exception

of the energy values for Pd 3d and Ga LMM signals, which are within a ±0.3 eV error owing to their lower signal-to-noise ratios.

The acquired spectra were processed with Microcal Origin® 4.1 and the XPSPEAK® 4.0 programs, as follows: A smoothing of the peaks was achieved using FFT, then a Shirley background was subtracted, and a Gaussian–Lorentzian sum function was used for fitting. XPS relative surface composition was calculated from photoelectron peak areas after deconvolution.

FT-IR Studies

Catalysts samples were pressed into wafers of 10 mg/cm^2 at 5 ton/cm^2. Previously, it was verified that the specific surface area of the catalysts is not decreased by this treatment. These self-supported wafers were placed in turn into a Pyrex cell with water-cooled NaCl windows, which was attached to a conventional high vacuum system (base pressure = 10^{-6} Torr), equipped with a manifold for gas flow. All catalysts pretreatments and IR measurements (transmission mode) were performed *in situ* at 760 Torr, except during evacuation.

Samples of the prereduced catalyst were heated form 298 to 723 K under O_2 flow (100 cm^3/min, 5 K/min) and promptly cooled to 343 K under vacuum. Next, H_2 was admitted into the cell (100 cm^3/min) and the temperature was increased to 723 K (5 K/min). After 30 min at this last condition the cell was evacuated for 20 min at 723 K. Then, the temperature was gradually decreased under vacuum to allow for reference IR spectra of the "clean wafers" to be taken, for reference background subtraction. It is important to emphasize that the prereduced catalysts had to be first oxidized under flowing oxygen to remove any remaining bands in the 3000- to 2800-cm^{-1} region. These spurious bands usually appear as a consequence of adventitious oil coming from the process of wafer preparation and they are attributed to the C–H stretching modes of CH_x groups.

A selected set of prereduced samples was first cleaned as described before and then gradually reduced from 298 to 723 K under flowing H_2 (100 cm^3/min, 5 K/min). After 15 min at this last condition a mixture of $H_2/D_2 = 1/1$ v/v (100 cm^3/min) was admitted into the IR cell for 15 min and, finally, the gas flow was switched to pure D_2 for another 15 min (100 cm^3/min). Reference spectra were taken after 20 min of evacuation at 723 K.

Finally, a sample of the calcined PdGa80 catalyst was treated in flowing H_2 (100 cm^3/min) after evacuating the cell for 15 min, as follows: (i) heating from 298 to 723 K (5 K/min); (ii) cooling, immediately, to 343 K (3 K/min); (iii) heating from 343 to 723 K (5 K/min); (iv) evacuating to the base pressure, for 20 min, at 723 K; and, finally, (v) cooling to room temperature. Again, IR spectra of the clean wafer were taken under this last cooling process for background subtraction.

A shimadzu 8210 FT-IR spectrometer with a DLATGS detector was used to collect the transmission spectra at 4-cm^{-1} resolution (100 scans). The Microcal Origin® 4.1 software (with Peak fitting module) was employed to correct the background spectra at each temperature and to measure peak areas and/or intensities.

Gases

AGA ultrahigh-purity grade H_2 (99.999%) and Ar (99.999%), research grade O_2 (99.999%), and high-purity N_2 (99.998%) were further purified prior to use. Hydrogen, argon, and nitrogen were passed through molecular sieve traps (3-A Fisher) and MnO/Al_2O_3 cartridges to remove water and oxygen impurities. Oxygen was passed through a molecular sieve trap (3-A Fisher) and Ascarite® to remove water and carbon dioxide, respectively.

RESULTS AND DISCUSSION

Effect of the Hydrogen Reduction on Pd and Ga Oxidation States

Table 2 summarizes the binding energy (BE) and kinetic energy (KE) values of the most relevant palladium and gallium signals, as a function of sample composition, for the treatments described under Experimental. As an example, the smoothened XPS spectra of Si 2p, Pd 3d, O 2s, and Ga 3d core levels and the Ga LMM Auger signal are illustrated in Fig. 1 for the PdGa40 precursor reduced *in situ* at 523 K.

For silicon, the Si 2p peak for all the samples and after each treatment was, within the experimental error, characteristic of SiO_2 (BE $\cong$ 103.1 eV, FWHM $\cong$ 2.4 eV) (20). Palladium $3d_{5/2}$ BE values for our catalysts calcined at 673 K were assigned to palladium(II) cations according to reference data (20, 22). It is well-known that metallic palladium binding energy values consistently larger than that of the bulk metal are obtained when metal crystallites smaller than approximately 4 nm are deposited on the surface of an insulator (22–25). Thus, Pd $3d_{5/2}$ peak positions for the catalysts reduced at $T \geq 573$ K, BE = 335.8–336.4 eV, correspond to ultradispersed, reduced palladium particles. A mixture of Pd^0 and Pd^{2+} was obtained over the clean or gallium-promoted Pd/SiO_2 at the lowest reduction temperature (423 K), at variance with our hydrogen-flowing temperature-programmed reduction (TPR) results, which indicated the complete reduction of Pd at 423 K (13). This disagreement might be due to an insufficient H_2 supply in the XPS pretreatment chamber and/or to a difference (estimated in about 50 K) between the measured temperatures of the catalysts sample under both diverse reduction treatments, as it is well-known that supported palladium oxide readily reduces at 393 K (26).

It is important to recall, now, that the average diameter of the palladium metal particles measured by TEM was almost

TABLE 2

XPS and Auger Results as a Function of Sample Composition and Treatments

Sample code	Treatment	T(K)	Binding energies (eV) Pd $3d_{5/2}$ Pd^0	Pd $3d_{5/2}$ Pd^{2+}	Ga 3d Ga^{3+}	Ga 3d $Ga^{\delta+a}$	Kinetic energy (eV) Ga $L_3M_{45}M_{45}$	Percentage reduced Pd^0	Percentage reduced $Ga^{\delta+a}$
PdGa00	Calcination	673[b]	—	337.4	—	—	—	0	—
	Reduction	423[b]	336.1	337.8	—	—	—	72	—
		723[b]	336.3	—	—	—	—	100	—
		523[c]	335.8	—	—	—	—	100	—
PdGa40	Reduction	723[d]	336.0	—	21.0	19.8	1060.3	100	23
		523[c]	335.8	—	20.7	19.5	1061.1	100	30
PdGa80	Calcination	673[b]	—	338.2	20.6	—	1061.2	0	0
	Reduction	423[b]	336.2	338.4	20.9	19.5	1061.0	66	16
		723[b]	336.4	—	21.0	19.6	1061.0	100	23
		523[c]	336.4	—	20.8	19.5	1061.6	100	31
Ga80	Calcination	673[b]	—	—	20.8	—	1060.4	—	0
	Reduction	423[b]	—	—	20.6	—	1060.4	—	0
		723[b]	—	—	21.1	19.6	1060.4	—	28
		523[c]	—	—	20.8	19.5	1061.5	—	25
Ga					18.7[e,f]		1068.1[e]	—	
Ga_2O					19.0[f]		—	—	
Ga_2O_3					20.5[e,f]		1062.4[e]	—	

[a] $\delta < 2$.
[b] A *precursor* sample was used as the starting material.
[c] A *prereduced catalyst* sample was used for this experiment: A sample of the precursor was calcined *ex situ* in flowing air at 673 K (2 h), prereduced in flowing H_2 at 723 K (2 h), and then reduced *in situ* (inside the XPS pretreatment chamber) in 400 Torr of H_2 at 523 K (30 min).
[d] A *precursor* sample was calcined *in situ* at 673 K in 400 Torr of static O_2, then reduced at 723 K in 400 Torr of static H_2, for 30 min each time.
[e] From Ref. (20).
[f] From Ref. (21).

identical for the whole set of the prereduced catalysts, in contrast with the decrease of the exposed metal fraction (FE) in the preparations where the gallium content was progressively increased (see Table 1). Concurrently with the TEM measurements, no trend was detected either for any chemical shift of the Pd 3d signal accompanying a higher loading of the promoter on the Pd/silica catalyst. Thus, an impact over the Pd chemical shift owing to the coverage of the palladium crystallites by gallium species cannot be seen by XPS. As a consequence, the reported Pd $3d_{5/2}$ BE values for Pd^0 in Table 2 should be consider indistinguishable.

The effects of the high-temperature reduction treatments over the supported gallium oxide appear fairly well in the XPS spectra: So, two shoulders for the Ga 3d core-level signal, which are partially overlapped with the O 2s photoelectron peak, can be already individualized upon reducing the PdGa40 precursor at 573 K (Fig. 1). More explicitly, the deconvoluted peaks of the O 2s and Ga 3d photoelectron lines for the Ga80 and PdGa80 precursors reduced at 723 K are shown on the rough XPS spectra in Fig. 2.

The most important feature to be emphasized is that the presence of these two Ga 3d lines, from now on defined as the high- and low-binding-energy components (HBE and LBE, respectively) of the Ga 3d signal, was consistently observed in all the gallium-containing catalysts that had been reduced *at least once* at 723 K.

It is clear that the calcination pretreatment of the catalyst precursors at 673 K produced only gallium(III) oxide on the silica, since bulk gallium nitrate thermally decomposes to Ga_2O_3 above 523 K (27). Hence, the high-energy peak (HBE) located at approximately 20.8 eV is assigned to supported Ga^{3+} species on the calcined materials, whether Ga/SiO_2 or $Ga–Pd/SiO_2$ (see Table 2).

After reduction in hydrogen at 723 K a new Ga 3d signal appeared at lower energy (LBE) at 19.6 eV for Ga/SiO_2. Separated TPR experiments indicated that incomplete reduction of Ga^{3+} on supported gallium on SiO_2 took place under similar conditions (13). Indeed, hydrogen-reduced bulk Ga_2O_3 and mechanical mixtures or impregnated ZSM-5 zeolite with Ga_2O_3 have yielded conclusive evidence of the partial reduction of gallium(III) species to probably Ga^{1+} cations (28–30). Upon reduction, the low-energy Ga 3d peak was also present on the gallium-promoted palladium catalysts, but it became visible at earlier temperatures, from 423 K onward, coincidentally with our previous TPR experiments. This last result is in

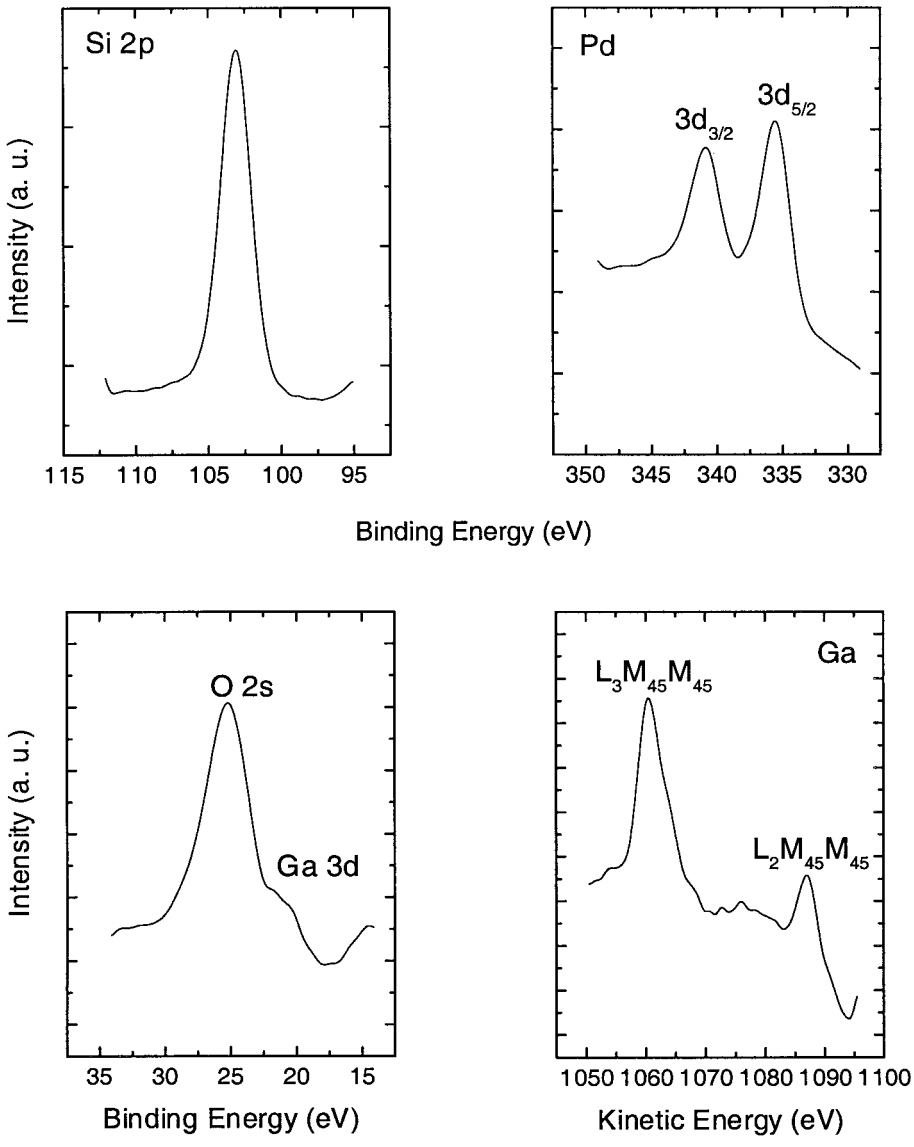

FIG. 1. XPS and Auger spectra of the PdGa40 precursor following calcination in O_2 at 637 K (30 min) and reduction in H_2 at 573 K for 30 min.

complete agreement with the suggested Pt promotion effect on the reduction of gallium(III) in Pt–Ga_2O_3/ZSM-5 by Shpiro *et al.* (29).

Other alternatives that might account for the appearance of the LBE band in our reduced Ga–Pd/SiO_2 materials are the formation of metallic gallium and/or Pd–Ga alloy, which cannot be ruled out completely for at least three reasons: (i) the chemical shift from Ga^{1+} (Ga_2O) to Ga^0 (metallic gallium) is only 0.3 eV, (ii) alloy formation could induce an additional chemical shift, and (iii) partial overlapping of the Ga 3d signal with O 2s peak introduces supplementary errors in the measurements of peak positions.

Although XPS detection of small amounts of this presumed alloy would be very difficult, there are two points that allow us to believe that gallium(III) species were not totally reduced to metallic gallium. First, because it is hard to think of a reduction from Ga^{3+} to Ga^0 at temperatures as low as 423 K in the Ga–Pd/SiO_2 catalysts, as this process needs much higher temperatures (27) and, second, because the LBE signal have the same position for Ga/SiO_2 and for Ga-promoted Pd/SiO_2 catalysts.

It is then logical to conclude that the Ga 3d LBE component of all our catalytic systems corresponds to $Ga^{\delta+}$ species ($\delta < 2$) originated from supported Ga_2O_x ($x < 2$), probably Ga^{1+} or gallium suboxide, Ga_2O.

It is interesting that the Ga 3d BE reference values for bulk gallium compounds, given in Table 2, are slightly lower than those for supported gallium species, but the opposite is true for KE Ga LMM signal. Although size effects in X-ray photoelectron spectroscopy have not been reported

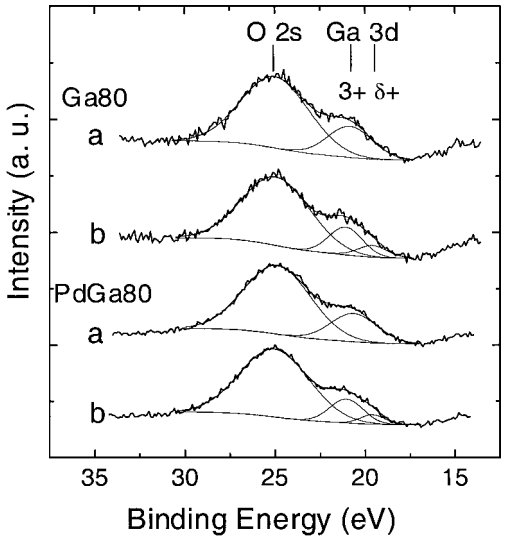

FIG. 2. Effect of H_2 reduction on the gallium XPS spectra of the Ga80 precursor (a) calcined at 673 K, then (b) reduced at 723 K, and of the PdGa80 precursor (a) calcined at 673 K, then (b) reduced at 723 K.

for metal oxide particles, it has been proved that the developing of a TiO_2–SiO_2 interface produces an up- and downshift in the Ti 2p XPS peak and the Ti Auger parameter ($\alpha' = BE_{Ti\,2p} + KE_{Ti\,LMV}$) (31–36), respectively. In our materials, regardless of the composition and treatment of the samples, average chemical shift (ΔBE) and Auger parameter shift ($\Delta\alpha'$) for gallium, of +0.3 and −1.0 eV, respectively (mainly produced by oxidized gallium, even under reducing conditions), with respect to bulk Ga_2O_3, can be calculated from Table 2.

The values of these shifts indicate changes in the extra-atomic relaxation energy rather than a variation of the initial state, when supporting gallium oxide (37, 38). In principle, differences in relaxation could be produced by crystal size and/or support effects. In our case, it is reasonable to expect that gallium species are mostly dispersed over the support, as a consequence of the impregnation and drying procedures used to prepare the samples (see next section). Furthermore, the occurrence of slightly higher BE values and lower Auger parameters for gallium oxides deposited over an insulator, compared to those for bulk gallium oxides, are consistent. It is possible to think, too, that at least a part of the gallium species are interacting via intimate contact with the support.

As for Si 2p photoelectron line, the O 2s peak was typical of silicon oxide (BE $\cong$ 25.0 eV, FWHM $\cong$ 4.2 eV) (20). We can then consider that the contribution from gallium oxides to this signal was negligible.

Quantification of the extent of Pd and Ga reduction was done after deconvoluting the Pd 3d and Ga 3d signals. The percentages of reduced Pd and Ga, defined as $[Pd^0/(Pd^0 + Pd^{2+})] \times 100$ and $[Ga^{\delta+}/(Ga^{\delta+} + Ga^{3+})] \times 100$, respectively, are reported in Table 2.

As expected, palladium(II) was fully reduced to metallic palladium upon heating either the calcined catalyst precursors or the prereduced Pd/SiO_2 or Ga–Pd/SiO_2 catalysts in 400 Torr of H_2 at 723 K, but the former materials (i.e., the calcined precursors) showed only partial reduction of the noble metal upon exposure to lower reduction temperatures. In fact, as was highlighted earlier, supported palladium oxide on silica can be completely transformed into finely dispersed metal particles under flowing hydrogen at temperatures as low as 423 K (13, 26). Again, an estimated difference of roughly 50 K between the real temperature of the catalysts pellets and the temperature measured by the thermocouple inside the XPS pretreatment chamber might well account for the apparent partial reduction of palladium in the precursors at this low-temperature reduction condition. Yet, the very close percentages of reduced palladium on PdGa00 (72%) and PdGa80 (66%) allow us to conclude that the presence of gallium had negligible effects over Pd reduction.

This was not quite true for the case of gallium. Dispersed gallium sesquioxide on silica was partially reduced to Ga_2O_x to different percentages depending on the reduction temperature and/or whether palladium was present or not. For PdGa80 a fraction of the gallium total (16%) was already reduced to $Ga^{\delta+}$ at 423 K, while for Ga80 no gallium ($\delta+$) species could be detected by XPS under this low-temperature reduction condition. The increase of the temperature to 723 K allowed further Ga_2O_x formation on both the Ga/SiO_2 and Ga–Pd/SiO_2 catalysts, but the percentage of reduced gallium ($Ga^{\delta+}$) was never higher than about a third of the total, using either precursors or the prereduced catalysts (span, 23–31%; Table 2).

An explanation of this promoting effect of palladium on the reduction of gallium(III) oxide could arise by taking into account hydrogen spillover. Palladium oxide starts reducing on silica at very low temperatures, lower than 373 K (26). The tiny metal crystallites that are formed in this first step are able to dissociate hydrogen molecules. Chemisorbed hydrogen atoms on Pd^0 spill over and reduce the closer Ga^{3+} cations at or above 423 K. However, this process needs further heating on the calcined Ga/SiO_2, since hydrogen activation of Ga_2O_x takes place at higher temperatures, as is discussed below.

Concerning the aggregation state of the active components of our catalysts, XRD experiments over prereduced catalysts of the highest gallium loading (Ga80 and PdGa80) confirmed the absence of palladium, gallium–palladium alloy, or gallium oxides particles bigger than 4 nm. Nishi *et al.* prepared SiO_2-supported Ga_2O_3 samples by impregnation of silica with an aqueous solution of gallium nitrate followed by evaporation and calcination in air at 823 K for 4 h (39). From 1.5 to 10.0 wt% Ga content, the size of their Ga_2O_3-supported particles, estimated by TEM, was between 2.0 and 6.2 nm. The existence of the poorly ordered ε-Ga_2O_3 crystal phase was suspected, from broad and weak XRD

peaks for gallium loading higher than 4.8 wt%, whereas amorphous gallium oxide prevailed for lower gallium contents (39). Hence, by no means do our XRD results contradict the data of Nishi and coworkers, since more drastic drying and calcination conditions were used in their experiments. We conclude, then, that finely dispersed mixed gallium oxides and/or metallic palladium are spread over the silica support on each of our reduced catalysts.

Gallium–Hydrogen Bond Formation as Detected by IR Spectroscopy

After exposing the prereduced gallium and gallium–palladium-containing catalysts to flowing hydrogen at 343 K, a low-intensity, broad IR bond at 3000 cm^{-1} together with an overlapped band corresponding to the ν(OH) band of interacting silanol groups via hydrogen bonding over the catalysts, at approximately 3550 cm^{-1}, were immediately formed. The source of these hydroxyl bands is mainly ascribed to water formation, from the reduction of palladium and gallium oxides which were produced during the cleaning process (oxidation step).

The intensity of the band at 3000 cm^{-1} increased with the total gallium loading on the catalysts, and it was absent on unpromoted Pd/SiO_2. Due to its proximity to the hydroxyl stretching bands, it was assigned to the stretching mode of interacting hydroxyl groups on the surface of gallium oxide particles.

Those ν(OH) bands, and the δ(OH) band at 1630 cm^{-1}, disappeared simultaneously after heating in hydrogen, as water was removed from the surface of the materials. Once at 723 K, it was possible to observe only a band at 3670 cm^{-1} in the gallium-containing catalysts (Fig. 3). Still, it was difficult to follow its evolution at temperatures lower than 700 K, due to its superposition with Si–OH bands. The band at 3670 cm^{-1} was assigned to the O–H stretching mode in Ga–OH or Si–O(H)–Ga, in agreement with other reported values (40–42). We assumed that this band is involved in the development or evolution of the main infrared signal at 2020 cm^{-1}, discussed in the following paragraphs.

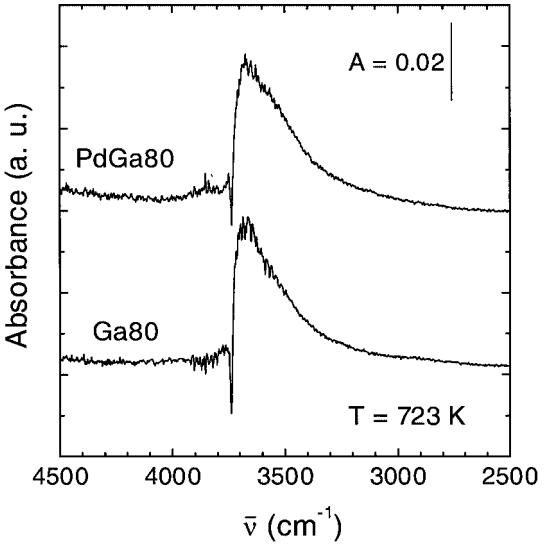

FIG. 3. Infrared spectra of the ν(OH) region under flowing H_2 (100 cm^3/min) at 723 K, for the prereduced catalysts Ga80 and PdGa80.

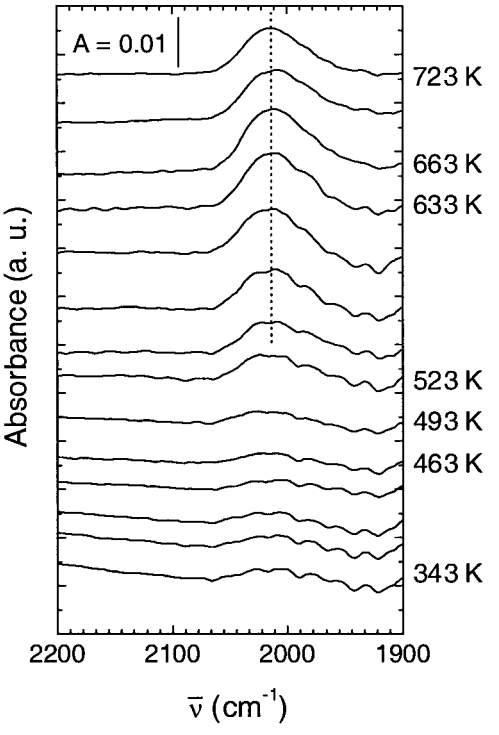

FIG. 4. Evolution of the $Ga^{\delta+}$–H stretching band (2020 cm^{-1}) over prereduced PdGa80 under flowing H_2 (100 cm^3/min), from 343 to 723 K. Heating rate = 5 K/min.

Figure 4 shows the formation of an infrared band at approximately 2020 cm^{-1} on prereduced $Ga–Pd/SiO_2$ with the highest total gallium content (PdGa80), upon heating the catalyst under flowing hydrogen. This band could be reliably measured against the background above approximately 500 K (2027 cm^{-1}). Its intensity grew up until 660 K and then leveled off at higher temperatures (2015 cm^{-1}).

A comparison of the intensity of this band with total gallium loading on Ga/SiO_2 and $Ga–Pd/SiO_2$ catalysts at 723 K under hydrogen is shown in Fig. 5. This figure discloses that Pd/SiO_2 is unable to form the surface species or bond responsible for the band at 2020 cm^{-1}. As for the other catalysts, it can be readily inferred that the only requisite for its development is the presence of gallium, because the band intensity is proportional to the Ga weight loading. Irrespective of the palladium content, the band position shifted from 2026 to 2015 cm^{-1} as the gallium loading went from 2.6 to 9.2 wt%. Due to the low intensity of this band in some cases, however, it was extremely relevant to pay close attention to

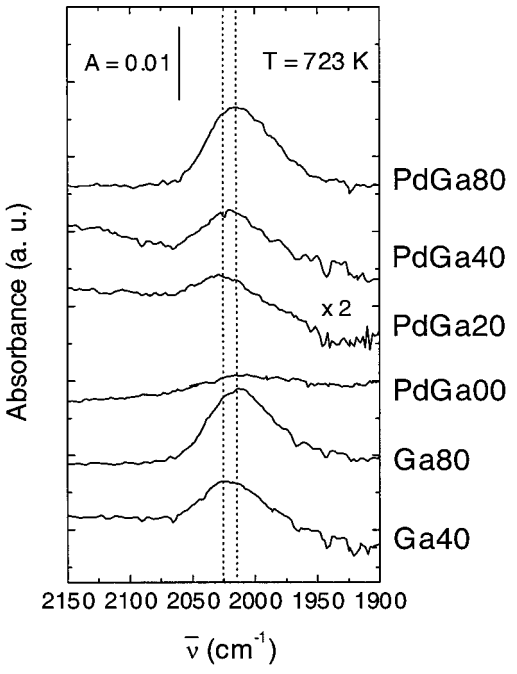

FIG. 5. Infrared spectra of the 2150- to 1900-cm^{-1} region at 723 K, for the full set of prereduced catalysts. Hydrogen flow = 100 cm^3/min.

this spectral region, which was accomplished by means of designated experiments, using H_2, D_2, and their mixtures, as discussed next.

The origin of the 2020-cm^{-1} band was attributed to gallium–hydrogen bond formation and was assigned to the stretching mode of $Ga^{\delta+}$–H, ν(Ga–H). Three aspects of all spectra we judge to be critical to the unambiguous identification of this assignment. The first one is related to the wavenumber position of this band when compared to molecular model systems, the second one to the relationship between the content of $Ga^{\delta+}$ species and the intensity of the ν(Ga–H) band, and the last to the wavenumber position of the peaks when performing H–D isotopic exchange experiments, as follows:

(i) The infrared spectra of pure and nonpure gallanes show different Ga–H bands, e.g., stretching, bending, torsion, and combination modes. Of those modes, only one stretching mode arises at wavenumbers higher than 1300 cm^{-1}, i.e., in our transparent region of infrared spectra, and this mode belongs, in particular, to a terminal Ga–H bond, $\nu(Ga–H_{terminal})$ or, hereafter, ν(Ga–H) (43–50). Table 3 summarizes the infrared band positions for this last mode in model systems. It shows that the ν(Ga–H) mode for gallanes lies between 2050 and 1800 cm^{-1}. Then, if $Ga^{\delta+}$–H is formed by reacting Ga_2O_x with hydrogen in our catalysts, no more than one band would be expected to show up at a wavenumber higher than 1800 cm^{-1} in our diagnostic region, as it is found.

Meriaudeau and Primet attributed their IR signal at 2020 cm^{-1} to Ga–H species over partially reduced α-Ga_2O_3, which is identical to our result regarding this infrared peak (40). To our knowledge, these authors reported the first and only evidence by a direct method of gallium–hydrogen bond formation on a material surface, which we corroborate on the surface of our catalysts.

(ii) The evolutions of the 2020-cm^{-1} peak intensity for all our prereduced catalysts versus temperature increase are displayed in Fig. 6. This band developed gradually while the temperature was raised, over both the Ga/SiO_2 and the Ga–Pd/SiO_2 catalysts. Then the band height flattened, from 660 K onward, keeping its maximum intensity value. This final intensity value ($T > 653$ K) increased with total gallium content in either the gallium or gallium–palladium-containing catalysts.

Figure 7 condenses this last finding and shows that the 2020-cm^{-1} peak intensity is directly proportional to the total gallium content (lower scale). Moreover, since the $Ga^{\delta+}$ fraction is almost the same when using different total gallium loading (see Table 2), these intensity values, as also shown in Fig. 7, have a linear relationship with the $Ga^{\delta+}$ loading, too (upper scale).

Similar behavior was observed for the O–H band at 3670 cm^{-1}, although the quantification had more random

TABLE 3

Infrared Peak Position of the Fundamental Stretching Mode of Terminal Ga–H Bond ν(Ga–H) in Model Systems[a]

Wavenumber (cm^{-1})	Model system[b]	Reference
Chlorine-containing compounds		
2047	Cl**HGa**(μ-Cl)$_2$**GaH**Cl	43
2020	**H_2Ga**(μ-Cl)$_2$**GaH$_2$**	44
Phosphorous-containing compounds		
1854	$H_3P \cdot$ **GaH$_3$**	45
1831	$Me_3P \cdot$ **GaH$_3$**	46, 47
Nitrogen-containing compounds		
1941 and 1809	[**H_2Ga**$(NH_3)_2$]$^+$ and **GaH_4^-** in [$H_2Ga(NH_3)_2$]$^+GaH_4^- \cdot 2NH_3$	45, 48
1839	$Me_3N \cdot$ **GaH$_3$**	45, 49
1790	$(Me_3N)_2$**GaH$_3$**	45
Alkyl-containing compounds		
1933	Et_2**GaH**, [Et**GaH$_2$**]$_2$ or Et_2**GaH** $\cdot$ OH_2	45
Pure gallane		
1993 and 1976 (vapor) 2015 and 1968 (trapped in an Ar matrix)	**H_2Ga**(μ-H)$_2$**GaH$_2$**	45, 50
2020	$Ga^{\delta+}$–H in α-Ga_2O_3	40

[a] The other Ga–H vibrational modes, e.g., $\nu(Ga–H_{bridge})$, $\rho(GaH_2$ or $GaH_3)$, $\delta(GaH_2$ or $GaH_3)$, and/or $\delta(GaH_{terminal})$, usually occur at substantially lower energy (wavenumber < 1300 cm^{-1}), i.e., outside our wavenumber window.

[b] Boldface indicates terminal Ga–H bonds.

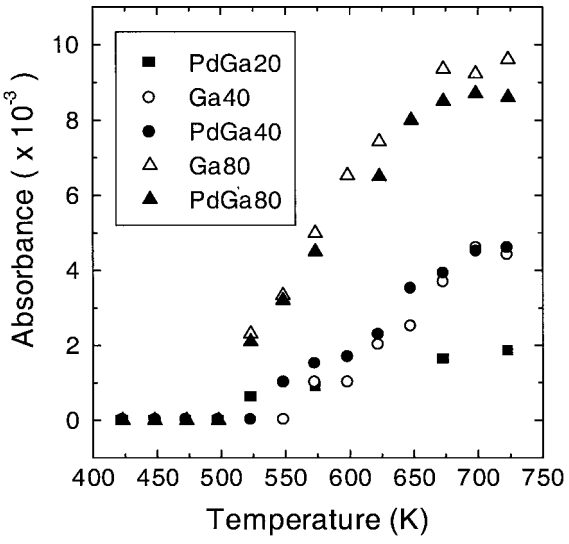

FIG. 6. Infrared intensity of the band corresponding to the stretching mode of the $Ga^{\delta+}$–H bond (2020 cm^{-1}) as a function of temperature, for prereduced gallium and gallium–palladium-containing catalysts. Hydrogen flow = 100 cm^3/min. Each point is the averaged intensity of three replicates, obtained in three separate measurements.

errors, owing to the overlapping with the O–H stretching mode of Si–OH groups.

(iii) The infrared spectra for H–D exchange experiments at 723 K are summarized in Fig. 8. After switching from H_2 to the H_2/D_2 equimolar mixture, a decrease in the intensity of the 2020-cm^{-1} band is observed, while a new band at 1450 cm^{-1} shows up in the gallium-containing samples (Ga80 and PdGa80) and, under pure D_2, only the 1450-cm^{-1} peak appears on these catalysts. The experimental value for the ratio between these wavenumbers is 1.39, which is the expected one for the ν(Ga–H) versus the ν(Ga–D) modes, i.e., 1.40. Similarly, the wavenumber ratio observed between the O–H and O–D bands at 3670 and 2709 cm^{-1}, respectively, was close to the theoretical value: 1.35 (experimental) vs 1.37 (theoretical). Therefore, these results prove unambiguously that the 2020-cm^{-1} signal corresponds to a hydrogen-containing species.

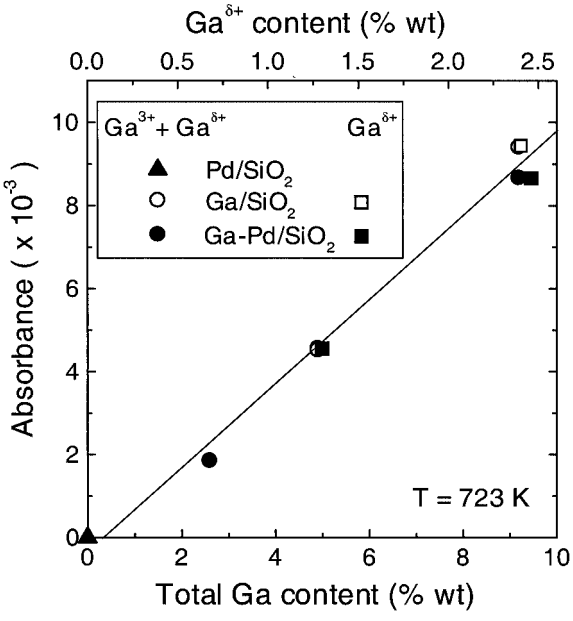

FIG. 7. Effect of gallium loading on the absorption intensity of the gallium–hydrogen bond signal, at 723 K. Hydrogen flow = 100 cm^3/min. Each point represents the average of three separate experimental runs.

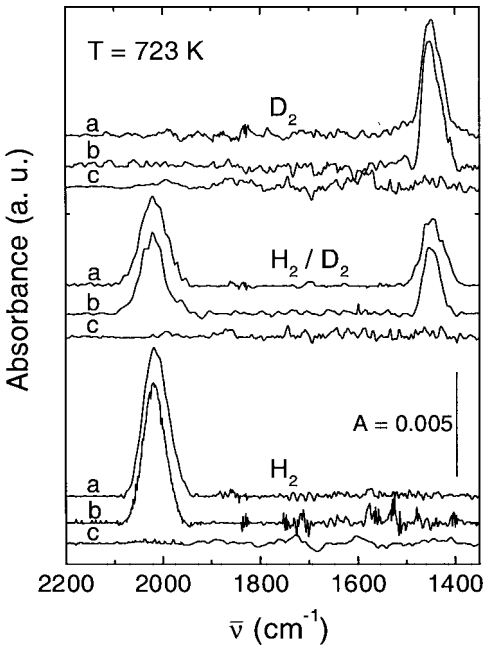

FIG. 8. Infrared spectra of the 2200- to 1350-cm^{-1} region of prereduced samples of (a) Ga80, (b) PdGa80, and (c) SiO_2 under gas flow (100 cm^3/min each) of pure H_2 (lower set of spectra), H_2/D_2 = 1/1 v/v mixture, and pure D_2 (upper set of spectra). Temperature = 723 K.

As mentioned above, the 2027-cm^{-1} infrared peak shifted downward to about −12 cm^{-1} when going from a low to a high loading of gallium, i.e., lower energy is required for the Ga–H bond vibration upon increasing the concentration of surface $Ga^{\delta+}$–H species over gallium or gallium–palladium catalysts (see Figs. 4 and 5).

We rule out the hypothesis of formation of surface GaH_x species ($x > 1$) which can cause this shift. If such multiple-hydrogenated species were formed, we would have expected that the observed change in wavenumber would not depend on gallium loading but rather on the amount of these new species produced upon increasing the reduction temperature. Also, for GaH_2 species two stretching modes, symmetric and antisymmetric, are predicted. Interaction among $Ga^{\delta+}$–H adspecies as the gallium loading (or the amount of this species) goes up is a more feasible

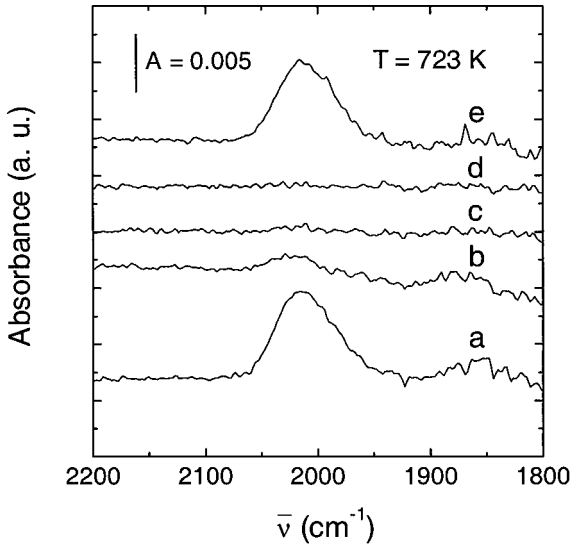

FIG. 9. Infrared spectra of the evolution of the ν(Ga–H) signal on the PdGa80 catalyst: (a) under flowing hydrogen (100 cm^3/min), then evacuating at 10^{-6} Torr for (b) 5, (c) 10, and (d) 15 min and (e) restoring the hydrogen flow (100 cm^3/min). Temperature = 723 K.

interpretation of the gradual small change of the wavenumber position for the ν(Ga–H) mode (static shift?) (51).

Now, the most controversial point seems to be the thermal stability of said $Ga^{\delta+}$–H species. On the one side, Meriaudeau and Primet (40) have postulated that the gallium–hydrogen bond formation mostly occurs by heterolytic cleavage of the hydrogen molecule, at least at 573 K, to yield Ga^{y+}–H ($y < 3$) and OH species: After heating precalcined α-Ga_2O_3 under 105 Torr of H_2 at 573 K, the 2020- and 3640-cm^{-1} bands appeared. The use of deuterium helped them to prove the assignments (40). Subsequently, Meriaudeau and Primet claimed that outgassing the sample at increasing temperatures from 323 K produced the decrease in these bands, which finally disappeared at 750 K. Owing to insufficient experimental details in their work (e.g., temperature of spectra acquisition and background subtraction, evacuation time, presumptive impurities in the samples that originated other high-frequency peaks at 3740 cm^{-1}), a direct comparison with our results is difficult. In particular, the duration of evacuation could be a crucial aspect. As Fig. 9 illustrates, upon outgassing our Ga–Pd/SiO_2 catalysts at 723 K (10^{-5} Torr), the 2020- and 3670-cm^{-1} peaks disappeared after 15 min. The same result was obtained over Ga/SiO_2 at 653 K. Meriaudeau and Primet observed similar behavior for bulk α-Ga_2O_3, but only at about 750 K (40). At lower temperatures, both infrared signals remained in their experiment, probably due to a fast scanning temperature under evacuation used by these authors. Also, it is possible to expect a different thermal stability for $Ga^{\delta+}$–H on the surface of a bulk Ga_2O_3 matrix compared to the silica-supported gallium oxide.

Nevertheless, it is more interesting to note the immediate redevelopment of the ν(Ga–H) and ν(O–H) bands after hydrogen flow restoration into the IR cell at 723 K (see Fig. 9). This result proves the reversibility of the reaction of $Ga^{\delta+}$–H bond formation. Moreover, the spectra did not differ significantly when the background subtraction of either the calcined or the prereduced sample was performed. Therefore, the gallium–hydrogen signal is undoubtedly removed after 15 min of evacuation. In other words, the $Ga^{\delta+}$–H bond breaks (or $Ga^{\delta+}$–H species decomposes) under evacuation at temperatures higher than 653 K.

On the other side, Meitzner *et al.*, studied the chemical state of gallium on a Ga/H–ZSM-5 catalyst by *in situ* X-ray absorption spectroscopy during the conversion of alkanes to aromatics (10). Under H_2, they proposed that Ga^{3+} cations were reduced to $Ga^{\delta+}$ (with δ between 0 and 1) at 780 K, suggesting the existence of gallium hydride monomeric species (GaH_x) coordinated to one or more basic framework oxygen within the zeolite channels. After cooling to room temperature, they found that those gallium species decomposed and suggested that this was the result of gallium oxidation to Ga^{3+}, probably by protons located at bridging hydroxyl and silanol groups, formed during the reduction step.

We believe that this might well be our case. Figure 10 shows the ν(Ga–H) band formation/decomposition over a sample of calcined PdGa80 catalyst. In the first step, the onset for Ga–H formation was approximately 523 K, although we know that gallium (3+) is partially reduced to gallium (δ+) at temperatures lower than 450 K

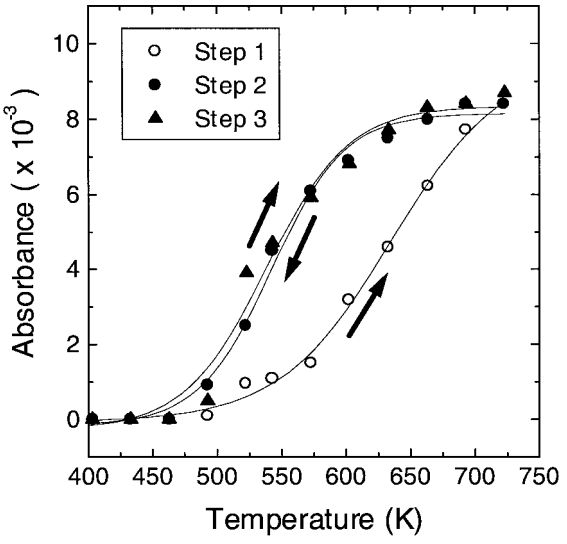

FIG. 10. Infrared intensity of the $Ga^{\delta+}$–H stretching band (2020 cm^{-1}) as a function of temperature, for a sample of calcined PdGa80. Experimental sequence: step 1, first heating slope; step 2, cooling slope; and step 3, second heating slope. The arrows indicate the direction of temperature variations (ascending, ↗; descending, ↙). Hydrogen flow = 100 cm^3/min.

when palladium is present (see XPS section). The intensity of this band increased up to 723 K. The second and third steps, cooling and heating the already reduced sample under hydrogen, exhibited an onset of the intensity of the $Ga^{\delta+}$–H stretching mode at approximately 473 K, i.e., at identical onset temperature and band development as those over prereduced samples, shown in Fig. 6.

An additional XPS experiment was made, introducing an outgassed sample of the prereduced and passivated PdGa80 catalyst, without further treatment, into the UHV chamber. The experiment showed that 20% of total gallium was in the reduced state (i.e., about 30% less than the *in situ* reduced precursor), indicating that our passivation treatment is able to keep most of the $Ga^{\delta+}$ ($\delta < 2$) under this low-oxidation state. This result was also confirmed in a separated TPR experiment over Ga80, which means that $Ga^{\delta+}$ species are stabilized probably by the support. The finding seems to be congruent with the stability of Ga^{1+} against oxidation in air up to ~773 K, as reported in Ga^{+}–β''–alumina and $GaZr_2(PO_4)_3$ by Wilkinson (52).

All together, these results may be rationalized by considering the following. Some authors have indicated, based on spectroscopic evidence, that gallium suboxide (Ga_2O) migration could explain the transfer of gallium from the outer into the channel system of zeolite matrices [e.g., in H–ZSM-5 (28–30) and faujasite zeolites (41)], upon hydrogen reduction. Truly, the sublimation temperature of bulk gallium suboxide (Ga_2O) is higher than 773 K (27, 53) but, on the other hand, it can be argued that the Tammann temperature of said suboxide is 603 K (29). Hence, our IR results using the calcined Ga–Pd/SiO_2 precursor suggest that during a first exposure to hydrogen, not only does Ga_2O_3 reduce to Ga_2O, next to Pd particles, but also the suboxide migrates to silica surface sites where $Ga^{\delta+}$ species could be stabilized by oxygen atoms of the support and could form Ga–H bonds (see Fig. 10, step 1). Once these reduced gallium cations are produced, they do not go back to their initial sites, making possible the evolution of $Ga^{\delta+}$–H species at lower temperatures upon H_2 exposure, and thus resembling the prereduced Ga/SiO_2 or Ga–Pd/SiO_2 catalysts. Therefore, the ν(Ga–H) IR signal in steps 2 and 3 of Fig. 10 exhibits the same evolution as in Fig. 6. For this to happen the hydrogen molecule is heterolytically cleaved to give SiO $\cdots$ Ga–H (2020 cm^{-1}) and SiO $\cdots$ Ga–OH (3670 cm^{-1}). This reaction is reversible, whether under evacuation or by just lowering the temperature. Reacting in this way, reduced gallium cations would disproportionate, changing their formal average oxidation state.

Finally, we conclude that our method of preparation of the gallium-promoted Pd/SiO_2 catalysts, including the prereduction and passivation treatments, is able to produce materials which are stable under air exposure and manipulation.

Role of Ga–H Formation over the Hydrogenation Catalytic Properties of Gallium

Two extra FTIR experiments were made, by increasing the temperature from 298 to 723 K at 3 K/min, under a flow of 100 cm^3/min of pure CO_2 or a H_2/CO_2 mixture ($H_2 : CO_2 = 3 : 1$) at 760 Torr fed into the infrared cell containing a sample of prereduced Ga40 catalyst cleaned *in situ* by reoxidization and reduction, as described under Experimental. Using pure CO_2, neither carbonates nor hydrogenated carbon species were detected by infrared spectroscopy within the temperature window, unlike the case of calcium-promoted Pd/SiO_2 (54). The usage of the reacting H_2/CO_2 mixture changed the picture dramatically, though. Already at 423 K bidentated formate species [$\nu_{as}(OCO) = 1598\ cm^{-1}$] were formed, and its amount went up to 600 K, paralleling the increase in intensity of the Ga–H stretching signal (Fig. 11). Above this last temperature the amount of surface formates decreased, giving rise to metoxi species [$\nu_{as}(CH_3O) = 2956\ cm^{-1}$ and $\nu_s(CH_3O) = 2858\ cm^{-1}$], while the amount of Ga–H bonds was kept almost unchanged. Thus, it is possible to posit that carbon dioxide hydrogenation takes place via H_2 dissociation by reduced gallium oxide (Ga_2O_x), forming $Ga^{\delta+}$–H species which are able to hydrogenate CO_2, stepwise, to formate and metoxi species.

Like for propane dehydrogenation over zeolite-supported gallium catalysts, we believe that gallium ($\delta+$) cations play a key role in hydrogenation catalytic reactions, particularly for the synthesis of oxygenated compounds from the hydrogenation of carbon oxides. The previous

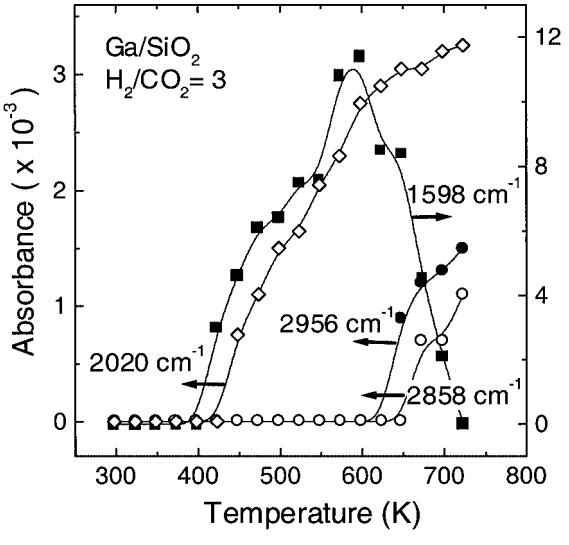

FIG. 11. Evolution of the infrared intensity of the ν(Ga–H) (2020 cm^{-1}), ν_{as}(OCO) (1598 cm^{-1}), $\nu_{as}(CH_3O)$ (2956 cm^{-1}), and $\nu_s(CH_3O)$ (2858 cm^{-1}) bands, during temperature-programmed reaction over the prereduced Ga40 catalyst using a H_2/CO_2 mixture (100 cm^3/min). Total pressure = 760 Torr. See Ref. (55) for band assignments.

results could readily explain the observed activity of Ga/SiO_2 to methanol and dimethyl ether from CO_2/H_2 at 553 K under high-pressure conditions (3 MPa) (13). Nevertheless, it is not straightforward to correlate just gallium–hydrogen bond development with methanol formation on gallium–palladium/silica catalysts, which are ~500-fold more active in this synthesis under pseudo-steady-state condition. Further infrared experiments showing the beneficial effect of gallium over palladium in carbon dioxide hydrogenation to methanol on these promoted catalysts will be reported shortly (56).

CONCLUSIONS

A palladium promotion effect was found on the reduction of silica-supported gallium(III) oxide. After the calcination of dried $Ga(NO_3)_3/SiO_2$ to Ga_2O_3/SiO_2, some Ga^{3+} cations were reduced to $Ga^{\delta+}$ ($\delta < 2$) upon heating in hydrogen at 723 K. However, a much lower temperature (<523 K) was required when both palladium and gallium were present on the support. This promotional effect is ascribed to spillover of atomic hydrogen from metallic palladium to close Ga^{3+} cations, as hydrogen activation by gallium oxide occurs at higher temperatures.

The most important band observed in the infrared spectra was located at 2020 cm^{-1}. This band appeared on both Ga/SiO_2 and $Ga–Pd/SiO_2$ catalysts and was assigned to the stretching mode of $Ga^{\delta+}$–H bond. A linear relationship between the intensity of this band and the content of reduced gallium was found. We suggest that the $Ga^{\delta+}$ cations, stabilized by coordination to oxygen atoms of the silica, are able to form gallium–hydrogen bonds over the surface of our supported catalysts, probably by heterolytical cleavage of the H_2 molecule to yield Ga–H and Ga–OH bonds simultaneously. Regardless of whether the materials contain palladium or not, the extent of gallium–hydrogen bond formation on prereduced catalysts in contact with H_2 starts at approximately 473 K and increases steadily until a plateau is reached over 653 K. The $Ga^{\delta+}$–H species are unstable below 450 K; they can be decomposed under evacuation at temperatures higher than 653 K but may be rapidly regenerated upon replenishing the H_2 atmosphere.

We believe that the hydrogenation–dehydrogenation capability of gallium-supported catalysts is closely related to the hydrogen dissociation unraveled by the Ga–H bond formation/decomposition that can be observed by FTIR. The behavior of these $Ga^{\delta+}$–H species demands that we carry out the catalytic reactions close to or inside their thermal stability region, to ensure their rapid formation/decomposition. Hence, the hydrogenation of carbon oxides to surface species can take place on Ga/SiO_2 only if $Ga^{\delta+}$–H species are formed, i.e., above 450 K. Higher temperatures allow this reaction to proceed to more hydrogenated intermediates which eventually desorb from the surface, as in the case of methanol synthesis.

ACKNOWLEDGMENTS

The financial support of the Universidad Nacional del Litoral (UNL), the Consejo Nacional de Investigaciones Científicas y Técnicas (CONICET), and the Agencia Nacional para la Promoción de la Ciencia y Tecnología (ANPCyT) is gratefully acknowledged. S. E. C. thanks Fundación Antorchas for the research fellowship received to do his work.

REFERENCES

1. Mowry, J. R., Anderson, R. F., and Johnson, J. A., *Oil Gas J.* **83**, 1288 (1985).
2. Kitagawa, H., Sendoda, Y., and Ono, T., *J. Catal.* **101**, 12 (1986).
3. Thomas, L. M., and Liu, X., *J. Phys. Chem.* **90**, 4843 (1986).
4. Gnep, N. S., Doyenet, J. Y., Seco, A. M., Ramoa Ribeiro, F., and Guisnet, M., *Appl. Catal.* **43**, 105 (1988).
5. Gnep, N. S., Doyenet, J. Y., and Guisnet, M., *J. Mol. Catal.* **45**, 281 (1988).
6. Meriaudeau, P., Sapaly, G., Wicker, G., and Naccache, C., *Catal. Lett.* **27**, 143 (1994); Mériaudeau, P., and Naccache, C., *J. Catal.* **157**, 283 (1995); Mériaudeau, P., and Naccache, C., *Catal. Today* **31**, 265 (1996).
7. Price, G. L., and Kanazirev, V., *J. Catal.* **126**, 267 (1990).
8. Buckles, G., Hutchings, J., and Williams, C. D., *Catal. Lett.* **8**, 115 (1991); Buckles, G., and Hutchings, J., *Catal. Lett.* **27**, 361 (1994).
9. Bàrre, M., Gnep, N. S., Magnoux, P., Sansare, S., Choudhary, V. R., and Guisnet, M., *Catal. Lett.* **21**, 275 (1993).
10. Meitzner, G. D., Iglesia, E., Baumgartner, J. E., and Huang, E. S., *J. Catal.* **140**, 209 (1993).
11. Inui, T., *Catal. Today* **29**, 329 (1996).
12. Fujitani, T., Saito, M., Kanai, Y., Watanabe, T., Nakamura, J., and Uchijima, T., *Appl. Catal. A* **125**, L199 (1995).
13. Bonivardi, A. L., Chiavassa, D. L., Querini, C. A., and Baltanás, M. A., *Stud. Surf. Sci. Catal.* **130D**, 3747 (2000).
14. Boccuzzi, F., Borello, E., Zecchina, A., Bossi, A., and Camia, M., *J. Catal.* **51**, 150 (1978).
15. Boccuzzi, F., Garrone, E., Zecchina, A., Bossi, A., and Camia, M., *J. Catal.* **51**, 160 (1978).
16. Lavalley, J. C., Saussey, J., and Raïs, T., *J. Mol. Catal.* **17**, 289 (1982).
17. Bonivardi, A. L., and Baltanás, M. A., *J. Catal.* **125**, 243 (1990).
18. Bonivardi, A. L., and Baltanás, M. A., *Thermochim. Acta* **191**, 63 (1991).
19. Fung, C. S., and Querini, C. A., *J. Catal.* **138**, 240 (1992).
20. Briggs, D., and Seah, M. P., *in* "Practical Surface Analysis," 2nd ed., Vol. 1, p. 609. Wiley, Surrey, 1990.
21. Carli, R., and Bianchi, C. L., *Appl. Surf. Sci.* **74**, 99 (1994).
22. Takasu, Y., Unwin, R., Tesche, B., and Bradshaw, A. M., *Surf. Sci.* **77**, 219 (1978).
23. Ryndin, Yu. A., Nosova, L. V., Boronin, A. I., and Chuvilin, A. L., *Appl. Catal.* **42**, 131 (1988).
24. Mason, M. G., *Phys. Rev. B* **27**, 748 (1983).
25. Kohiki, S., *Appl. Surf. Sci.* **25**, 81 (1986).
26. Anderson, J. R., "Structure of Metallic Catalysts." Academic Press, Bristol, 1975.
27. Hutter, J.-C., *in* "Noveau Traité de Chimie Minerale" (P. Pascal, A. Chrétieu, Y. Trambouze, J.-C. Hutter, and W. Freundlich, Eds.), Tome IV, p. 669. Maisson et Cie., Paris, 1961.
28. Carli, R., Bianchi, C. L., Giannantonio, R., and Ragaini, V., *J. Mol. Catal.* **83**, 379 (1993).
29. Shpiro, E. S., Shevchenko, D. P., Kharson, M. S., Dergachev, A. A., and Minachev, Kh. M., *Zeolites* **12**, 670 (1992).

30. Kanazirev, V., Price, G. L., and Tyuliev, G., *Zeolites* **12**, 846 (1992).
31. Fernández, A., Caballero, A., and González-Elipe, A. R., *Surf. Interface Anal.* **18**, 392 (1992).
32. Lassaletta, G., Fernández, A., Espinós, J. P., and González-Elipe, A. R., *J. Phys. Chem.* **99**, 1484 (1995).
33. Lassaletta, G., Fernández, A., and González-Elipe, A. R., *J. Electron Spectrosc. Relat. Phenom.* **87**, 61 (1997).
34. Stakheev, A. Yu., Shpiro, E. S., and Apijok, J., *J. Phys. Chem.* **97**, 5668 (1993).
35. Ingo, G. M., Diré, S., and Babonneau, F., *Appl. Surf. Sci.* **70/71A**, 230 (1993).
36. Mejías, J. A., Jiménez, V. M., Lassaletta, G., Fernández, A., Espinós, J. P., and González-Elipe, A. R., *J. Phys. Chem.* **100**, 16255 (1996).
37. Wagner, C. D., *Faraday Discuss. Chem. Soc.* **60**, 291 (1975).
38. Wagner, C. D., and Joshi, A., *J. Electron Spectrosc. Relat. Phenom.* **47**, 283 (1988).
39. Nishi, K., Shimizu, K., Takamatsu, M., Yoshida, H., Satsuma, A., Tanaka, T., Yoshida, S., and Hattori, T., *J. Phys. Chem. B* **102**, 10190 (1998).
40. Meriaudeau, P., and Primet, M., *J. Mol. Catal.* **61**, 227 (1990).
41. Sulikowski, B., Olejniczak, Z., and Cortéz Corberán, V., *J. Phys. Chem.* **100**, 10323 (1996).
42. Meriaudeau, P., and Naccache, C., *Appl. Catal.* **73**, L13 (1991).
43. Beachley, O. T., Jr., and Simmons, R. G., *Inorg. Chem.* **19**, 783 (1980).
44. Goode, M. J., Downs, A. J., Pulham, C. R., Rankin, D. W. H., and Robertson, H. E., *J. Chem. Soc. Chem. Commun.* 768 (1988).
45. Pulham, C. R., Downs, A. J., Goode, M. J., Rankin, D. W. H., and Robertson, H. E., *J. Am. Chem. Soc.* **113**, 5149 (1991).
46. Greenwood, N. N., Ross, E. J. F., and Storr, A., *J. Chem. Soc.* 1400 (1965).
47. Odom, J. D., Chatterjee, K. K., and Durig, J. R., *J. Phys. Chem.* **84**, 1843 (1980).
48. Shirk, A. E., and Shriver, D. F., *J. Am. Chem. Soc.* **95**, 5904 (1973).
49. Durig, J. R., Chatterjee, K. K., Li, Y. S., Jalilian, M., Zozulin, A. J., and Odom, J. D., *J. Chem. Phys.* **73**, 21 (1980).
50. Downs, A. J., Goode, M. J., and Pulham, C. R., *J. Am. Chem. Soc.* **111**, 1936 (1989).
51. Hammaker, R. M., Francis, S. A., and Eischens, R. P., *Spectrochim. Acta* **21**, 1295 (1965).
52. Wilkinson, A. P., *Inorg. Chem.* **36**, 1602 (1997).
53. Lide, D. R., Ed., "Handbook of Chemistry and Physics," 72nd ed. CRC, Boca Raton, FL, 1991.
54. Cabilla, G. C., Doctoral thesis. Universidad Nacional del Litoral, Argentina, 2000.
55. Cabilla, G. C., Bonivardi, A. L., and Baltanás, M. A., *J. Catal.* **201**, 213 (2001).
56. Collins, S. C., Baltanás, M. A., and Bonivardi, A. L., manuscript in preparation.